Published in final edited form as:
Photochem Photobiol. 2010 ; 86(3): 563–570. doi:10.1111/j.1751-1097.2010.00719.x.

One-electron oxidation of a pyrenyl photosensitizer covalently attached to DNA and competition between its further oxidation and DNA hole injection

Byeong Hwa Yun[1], **Peter C. Dedon**[2], **Nicholas E. Geacintov**[1], and **Vladimir Shafirovich**[1,*]

[1]Chemistry Department and Radiation and Solid State Laboratory, New York University, 31 Washington Place, New York, New York 10003-5180

[2]Biological Engineering Division, Massachusetts Institute of Technology, Cambridge, Massachusetts 02139

Abstract

The photosensitized hole injection and guanine base damage phenomena have been investigated in the DNA sequence, 5′-d(CAT$\mathbf{G_1^{Py}}$C$\mathbf{G_2}$TCCTAC) with a site-specifically positioned pyrene-like (Py) benzo[*a*]pyrene 7,8-diol 9,10-epoxide – derived N^2-guanine adduct (G_1^{Py}). Generation of the Py radical cation and subsequent hole injection into the DNA strand by a 355 nm nanosecond laser pulses (~4 mJ/cm^2) results in the transformation of G_1^{Py} to the imidazolone derivative Iz_1^{Py} and a novel G_1^{Py*} photoproduct that has a mass larger by 16 Da (M+16) than the mass (M) of G_1^{Py}. In addition, hole transfer and the irreversible oxidation of G_2, followed by the formation of Iz_2 was observed (Yun et al., *J. Am. Chem. Soc.***2007**, 129, 9321). Oxygen-18 and Deuterium isotope labeling methods, in combination with an extensive analysis of the MS/MS fragmentation patterns of the individual dG^{Py*} nucleoside adduct and other data, show that dG^{Py*} has an unusual structure with a ruptured cyclohexenyl ring with a carbonyl group at the rupture site and intact guanine and pyrenyl residues. The formation of this product competes with hole injection and thus diminishes the efficiency of oxidation of guanines within the oligonucleotide strand by at least 15% in comparison with that in the dG^{Py} nucleoside adduct.

Introduction

Benzo[*a*]pyrene, an extensively studied pre-carcinogenic polycyclic aromatic hydrocarbon (1), is metabolized by cytochrome P450 enzymes to highly reactive diol epoxides, including the biologically significant intermediate (+)-7*r*,8*t*-dihydroxy-9*t*,10*t*-epoxy-7,8,9,10-tetrahydrobenzo[*a*]pyrene (*anti*-BPDE) (2). This diol epoxide forms covalent adducts with DNA by binding predominantly to the exocyclic amino group of guanine via its C-10 position. The addition of the N^2-guanine to the C-10 position of BPDE can occur either by *cis* or *trans* mechanisms, thus forming two stereoisomeric adducts (3). The (+)-*trans*-addition product is the major adduct found in cellular DNA (4), and is designated as 10*S* (+)-*trans*-*anti*-[Py]-N^2-dG, or dG^{Py} (Figure 1). We have been studying the structural and functional characteristics of such lesions site-specifically inserted into oligonucleotides of defined sequence context for some time (5-8). The (+)-*trans* and stereochemically similar adducts have pyrene (Py)-like spectroscopic properties (9) with a strong absorption maximum in the 300 – 350 nm region and a fluorescence emission in the 390 – 440 nm region. The fluorescence of this product is strongly quenched by a photoinduced electron transfer mechanism (10-12). The nature of the electron transfer mechanism was investigated in detail

*To whom correspondence should be addressed: vs5@nyu.edu.

by laser flash photolysis methods that showed that the photoexcited Py residue can oxidize the adjacent guanine residue; the ion radical pair thus formed recombines non-radiatively, thus accounting for the observed fluorescence quenching (12-14). The spectroscopic properties of the G^{Py} adduct embedded in DNA have been used extensively to study the conformational properties of these lesions (15-17).

More recently we have used the G^{Py} adduct site-specifically incorporated into the oligonucleotide 5′-d(CAT**G_1^{Py}**C**G_2**TCCTAC) as a photosensitizer to inject holes into this sequence and to monitor oxidative damage at the Py-modified base, dG_1^{Py}, and the single, more distant unmodified guanine residue G_2 (18). The Py residue was selectively photoexcited with 355 nm nanosecond laser pulses (~4 mJ/cm^2) that generated the $Py^{\bullet+}$ radical cation by a two-photon induced ionization mechanism, as well as hydrated electrons that were trapped by molecular oxygen to form superoxide anions, $O_2^{\bullet-}$ (18).

Transient absorption spectroscopy methods were utilized to ascertain that $Py^{\bullet+}$ selectively oxidized the guanine residue to which it is attached (19); this is equivalent to 'hole injection' into the oligonucleotide (18) that results in the formation of the Py-modified guanine radical cation, $(G_1^{Py})^{\bullet+}$ (18, 19). These radical cations rapidly deprotonate to form the neutral guanine radicals bearing Py residues, $G_1^{Py}(-H)^{\bullet}$ radicals. The latter decay by at least two competitive mechanisms: (1) an electron transfer mechanism that generates the $G_2(-H)^{\bullet}$ radical that becomes irreversibly oxidized (18), or (2) transformation of $G_1^{Py}(-H)^{\bullet}$ to various oxidized products that included 2,5-diamino-4*H*-imidazolone lesions bearing pyrenyl residues (Iz_1^{Py}), generated by the combination of $G_1^{Py}(-H)^{\bullet}$ radicals with superoxide anion radicals (Figure 1). A previously unknown lesion, G_1^{Py*}, with a mass (M +16), which is by 16 Da greater than the mass (M) of the parent G_1^{Py}, was also detected in the irrradiated oligonucleotide d(CAT**G_1^{Py}**C**G_2**TCCTAC). These competitive reaction pathways are summarized in Figure 1. The formation of this product competes with hole injection and thus diminishes the efficiency of oxidation of guanines within the oligonucleotide strand.

The mass M + 16 is frequently associated with the formation of 8-oxo-7,8-dihydro-2′-deoxyguanosine (8-oxodG) lesions, a common oxidation product of guanine (20). In order to investigate this possibility, the M+16 oxidation product dG_1^{Py*} was excised from the oligonucleotide by enzymatic digestion methods, and the properties of the dG_1^{Py*} nucleoside were compared to those of the authentic *anti*-[Py]-N^2-8-oxodG adduct standard, 8-oxodG^{Py} (18). However, the chromatographic properties of the M+16 product dG_1^{Py*} were different from those of the 8-oxodG^{Py} standard, thus ruling out this possibility and the nature of this product was not further investigated.

In this work we investigated the structure of the dG_1^{Py*} product in detail by mass spectrometric MS/MS and spectroscopic methods. Our MS/MS studies were facilitated by generating larger quantities of the dG^{Py*} nucleoside standard than was possible by enzymatically digesting the photoirradiated oligonucleotide 5′-d(CAT**[G_1^{Py*}]**C**G_2**TCCTAC). The structure of this M+16 dG^{Py*} nucleoside standard was established by LC-MS/MS methods using ^{18}O and deuterium isotope labeling methods and analysis of the fragmentation patterns. We conclude that the M+16 nucleoside product represents an oxidized form of the photosensitizing dG_1^{Py} moiety that has an unusual structure with a ruptured cyclohexenyl ring, that leaves the guanine and pyrenyl residues remain intact. The formation of this product competes with hole injection and thus diminishes the efficiency of oxidation of guanines within the oligonucleotide strand.

Experimental

Materials

All chemicals (analytical grade) were used as received. The 10*S* (+)-*trans-anti*-[Py]-N^2-dG adduct dG^{Py} was synthesized by a direct reaction of dG with racemic *anti*-BPDE obtained from the National Cancer Institute Chemical Carcinogen Reference Standard Repository. The dG^{Py} products were isolated and purified by reversed-phase HPLC methods as previously described (3). The structure of the adduct was confirmed by LC-MS/MS methods and circular dichroism analysis.

Photochemical synthesis of the M+16 dG^{Py*} nucleoside adduct

A 25 nmol sample of the 10*S* (+)-*trans-anti*-[Py]-N^2-dG nucleoside in 0.25 mL air-equilibrated phosphate buffer solutions (pH 7) was photolysed by a train of 355 nm nanosecond Nd:Yag laser pulses (4 mJ/cm^2, 10 Hz) for 20 s. This procedure was repeated with fresh samples of the nucleoside in order to accumulate sufficient amounts for detailed analysis. The end products thus obtained were separated by reversed-phase HPLC methods. Typical elution conditions included a 0 – 15% linear gradient of solvent A (1:1 mixture of solvent B and water) in solvent B (3:1 mixture of methanol and acetonitrile) for 60 min, was employed a flow rate of 1 mL/min. The products were detected by their absorbance at 260 nm. Under these conditions the M+16 nucleoside eluted after 10.6 min, and the unmodified nucleoside G^{Py} eluted at 14.5 min. The HPLC fractions containing the M+16 adduct were evaporated under vacuum to remove organic solvent and were purified by a second HPLC cycle. The purified M+16 adducts were desalted by reversed-phase HPLC using the following mobile phases: 5 mM ammonium acetate (10 min), deionized water (10 min), and an isocratic 50 : 50 methanol and H_2O mixture (15 min), and then subjected to LC-MS/MS analysis.

LC-MS Assay

The end products of the 10*S* (+)-*trans-anti*-[Py]-N^2-dG photolysis were identified using an Agilent 1100 Series capillary LC/MSD Ion Trap XCT and an Agilent 1100 Series LC/MSD VL mono quadrupole mass spectrometer equipped with an electrospray ion source. In typical ion trap experiments 1 – 8 μL of the sample solutions were injected in a narrow bore Zorbax SB-C8 column (50 × 2.1 mm i. d.) and eluted with an isocratic mixture of methanol and water (55 : 45) with 0.1% formic acid as the mobile phase, at a flow rate of 0.25 mL/min. In mono quadrupole experiments, 10 – 30 μL of the sample solutions were injected into a Zorbax SB-C8 column (150 × 4.6 mm i. d.) and eluted with an isocratic mixture of methanol and water (55 : 45) with 0.1% formic acid as the mobile phase at a flow rate of 0.5 mL/min.

Results and Discussion

The 5′-d(CAT$\mathbf{G_1^{Py}}$C$\mathbf{G_2}$TCCTAC) oligonucleotide was dissolved in air-equilibrated phosphate buffer solutions (pH 7.0) and irradiated with 355 nm nanosecond laser pulses (~4 mJ/cm^2). The photoproducts were isolated by reversed-phase HPLC and identified by LC-MS methods. In HPLC separations of the products of photolysis, the major end product with a mass of M+16, eluted at 22 min which is greater by 16 Da than the mass of the parent adduct (M), which elutes at 28 min (typical results are shown in (18)). The product with mass (M-39) eluted at 24 min was formed in smaller quantities and was identified as the imidazolone dIz^{Py} product bearing an intact Py residue. The dG_1^{Py*} nucleoside product was isolated by enzymatic digestion of the irradiated oligonucleotide d(CAT$\mathbf{G_1^{Py}}$C$\mathbf{G_2}$TCCTAC). Its MS/MS properties were identical to those of an M+16 dG^{Py*} nucleoside product obtained by the photolysis, using identical irradiation conditions, of the

10*S* (+)-*trans-anti*-[Py]-N^2-dG nucleoside adduct, dG^{Py} (data not shown). The photolysis of the dG^{Py} nucleoside also generated the nucleoside dIz^{Py}. Thus the same products are formed within the oligonucleotide as at the nucleoside level, and we conclude that $dG_1{}^{Py*}$ is the same as the M+16 dG^{Py*} nucleoside standard. In addition to the Iz and M+16 oxidation products, laser pulse excitation induces the detachment of the pyrenyl residues. The formation of unmodified oligonucleotides with intact G replacing the adduct G^Py was clearly observed by gel electrophoresis methods (18, 21). The unmodified oligonucleotides were isolated by reversed-phase HPLC and identified by MALDI-TOF/MS methods (data note shown). In our typical experiments, the yields of the unmodified sequences were in the range of 0.5 – 0.6 %. The laser pulse – induced detachment of Py with similar yields was also observed in the case of the dG^{Py} nucleoside adducts.

Irradiation of either the nucleoside dG^{Py} or the oligonucleotide 5′-d(CAT**[G_1^{Py}]**C**G_2**TCCTAC) under the same conditions of laser energy and irradiation time generates the same amounts of the M+16 products with yields of 8%, as shown in Figure 2. The recovery of the unreacted dG^{Py} (67±7 %) is somewhat greater than that of the unmodified oligonucleotide 5′-d(CAT**[G_1^{Py}]**C**G**TCCTAC) (57±6 %); this relatively small difference was not further investigated.

The formation of M+16 product at $dG_1{}^{Py}$ competes with the formation of the $dG_1{}^{Py}(-H)^{\bullet}$ radical, which is equivalent to hole injection into the oligonucleotide. The $dG_1{}^{Py}(-H)^{\bullet}$ radical decays by competitive pathways to dIz^{Py} and an electron transfer step from $dG_1{}^{Py}(-H)^{\bullet}$ to G_2 that can result in the latter's irreversible oxidation. These competitive pathways are summarized in Figure 1. From Figure 2, it is evident that the oxidation of the Py photosensitizing moiety that results in the formation of the M+16 oxidation product $dG_1{}^{Py*}$ diminishes the yield of hole injection by ~ 15%. These results demonstrate that the oxidation of the photosensitizer can limit the efficiency of hole injection, and that a complete understanding of photoinduced hole injection and electron transfer phenomena in DNA should include information about the fates of the photosensitizing moieties and their chemical and photochemical stabilities. In our case, the $dG_1{}^{Py*}$ retains its photosensitizing properties that can lead to the near complete degradation of oligonucleotides (10, 18, 21). In the following, we establish the nature of the primary photoproduct M+16 dG^{Py*} product and propose a mechanistic pathway of its formation.

The ^{18}O and D isotope labeling of the dG^{Py*} nucleoside adducts

The difference in the masses of dG^{Py*} and dG^{Py}, is most likely associated with the insertion of an oxygen atom (16 Da) into the parent adduct. In oxidative processes, the sources of O atoms are typically either molecular oxygen or water molecules. Typically, the insertion of O-atoms into organic molecules (RH) to form ROH products, results in the appearance of one solvent-exchangeable proton. An example is the hydroxylation of the pyrenyl ring system induced by the photolysis of pyrene in oxygenated aqueous solutions (22). In this reaction, the insertion of each O-atom in the aromatic ring to form OH group results in the appearance of an additional exchangeable proton. In our experiments, we tracked the insertion of O-atoms into dG^{Py} using ^{18}O and deuterium isotope labeling experiments.

We synthesized the dG^{Py*} nucleoside in $H_2{}^{18}O$ solutions equilibrated with air containing normal molecular oxygen, $^{16}O_2$. The molecular ion, $[M+H]^+$ of the adduct is observed at *m/z* 588.2 (Figure 3A) that is by 2 Da greater than the control dG^{Py*} product (mass M+16) generated in the same manner in $H_2{}^{16}O$ solution (Figure 3B). This mass difference of 18 Da relative to the parent dG^{Py} adduct at *m/z* 570.2 (Figure 3E), provides straightforward evidence that the oxygen atom originates from $H_2{}^{18}O$ and not from $^{16}O_2$.

The numbers of exchangeable protons in the dG^{Py*} oxidation product were determined from the mass spectra after proton exchange in D_2O (99.9%) by repeated lyophilization, followed by redissolving the products in D_2O (Figures 3C and 3D). Using D_2O/acetonitrile mixtures as the mobile phase in LC-MS analysis, we found that the molecular ions of dG^{Py*} and dG^{Py} are observed at *m/z* 594.2 (Figure 3C) and *m/z* 578.2, respectively (Figure 3D). In contrast, LC-MS analysis in H_2O/acetonitrile mixtures yields *m/z* 586.2 (Figure 3B) and *m/z* 570.2 ions (Figure 3E), respectively. These differences in *m/z* values correspond to substitution of seven exchangeable H^+ for seven D^+ ions, plus one extra D^+ ion to generate the positively charged molecular ion. This observation allows to exclude hydroxylation of the pyrenyl ring as a potential mechanism of O-atom addition to the dG^{Py} nucleoside, as suggested in our previous report (18).

Circular dichroism spectra of the dG^{Py*} nucleoside adduct

Photooxidation of the 10*S* (+)-*trans-anti*-[Py]-N^2-dG to form the dG^{Py*} product is associated with significant changes in the circular dichroism spectra as shown in Figure 4. However, the absorption spectra of the dG^{Py} and dG^{Py*} are very close to one another, indicating that the Py residue is intact in the dG^{Py*} oxidation product. To explain these dramatic changes in the CD spectra, we propose that the photooxidation of the dG^{Py} adduct induces a cleavage of the non-aromatic cyclohexenyl ring. The opening of the aliphatic ring leads to changes in the relative orientations of the guanosyl and the pyrenyl residues while maintaining nearly unchanged absorption spectra; nevertheless, the 3 nm blue shifts in the absorption maxima of dG^{Py*} product suggest weaker Py – dG base stacking interactions (inset in Figure 4). The cyclohexenyl ring-opening leads to diminished orientation-dependent dipole-dipole interactions and thus a weakening of the CD spectra in the dG^{Py*} adduct. In the non-oxidized dG^{Py} nucleoside adduct, extensive dipole-dipole interactions result in a strong exciton coupling between these two moieties and thus the strong CD spectrum of the (+)-*trans-anti*-[Py]-N^2-dG adduct (23, 24). In this ring-opened structure, the guanosyl residue can assume different conformations because of the greater number of torsional degrees of freedom, in contrast to the intact (+)-*trans-anti*-[Py]-N^2-dG adduct that is conformationally severely constrained by steric hindrance effects (5, 6).

Rupture of the cyclohexenyl ring is required to form the dG^{Py*} adduct

Formation of the G^{Py*} product from the parent G^{Py} adduct by photocleavage of the cyclohexenyl ring is a unique pathway that can account for all of the experimental observations: (1) The difference in mass of 16 Da between dG^{Py*} and dG^{Py}, (2) The insertion of an O-atom from $H_2{}^{18}O$ without increasing the number of exchangeable protons, (3) The dramatic changes in CD spectra, and (4) The conservation of the intact G and the aromatic Py ring system in the dG^{Py*} adduct. There are examples of photochemical reactions, which involve heterolytic C-C bond cleavage in primary photochemical reaction steps, e.g., the photodecarboxylation of arylacetate ions (25), photodeformylation of 9-fluorene and 9-xanthenemethanols (26), and the photo-retro-aldol type processes of nitrophenylethyl alcohols (27, 28). Photoexcitation of these compounds in aqueous solutions induces heterolytic cleavage of the benzylic bonds to form the carbanion and carbocation-equivalent fragments, which immediately react with water to form end products. For instance, the UV photolysis (300 – 350 nm) of 2-(4-nitrophenyl)-l-phenylethanol in aqueous solutions generates 4-nitrotoluene and benzaldehyde products arising from the heterolytic cleavage of the benzylic bond in the parent compound (27). Here, we propose that the photoinduced heterolytic cleavage of the “benzylic” C9-C10 and C7-C8 bonds can initiate the formation of the M+16 products (Figure 5). The molecules **1** and **2** can be generated by cleavage of the C9-C10 bond and O-atom addition to either C10 (**1**) or C9 (**2**), whereas the molecules **3** and **4** can be produced by cleavage of the C7-C8 bond followed by O-atom addition to C7 (**3**) or C8 (**4**), respectively. The molecules **1** – **4** have intact G and Py

moieties, one additional O-atom (in the form of the carbonyl group), and the same number of exchangeable protons as the parent dG^{Py} adduct. Additional support for the dG^{Py*}cyclohexenyl ring cleavage was obtained by analysis of the fragmentation patterns of the M*+16 product observed in the positive product ion mode.

Positive product ion spectra

Representative positive product ion spectra of the dG^{Py*} adduct are shown in Figure 6. Fragmentation of the molecular ion, $[M+H]^+$ detected at *m/z* 586.2 induces the detachment of the sugar residue (−116 Da) to form the aglycone ion, $[BH_2]^+$ observed at *m/z* 470.1. The later ion is further fragmented by three pathways: (1) detachment of the pyrenyl residue to form the protonated guanine, $[GH]^+$ at *m/z* 152.2 (29), (2) expulsion of H_2O from the former cyclohexenyl ring to form the ion at m/z 451.1, and (3) cleavage of the pyrimidine ring of the guanine residue. The latter involves breakage of the C5 – C6 and N3 – C2 bonds to form the ion detected at *m/z* 394.2. This fragmentation mode of the pyrimidine ring has been detected in the 4-aminobiphenyl-N^2-dG adducts (30). The above fragmentation pathways are shown in Figure 7 for structure **1** (Figure 5), which is the most probable photoproduct (see, below). Thus, the product ion spectra support our hypothesis that the G and Py residues remain intact in the dG^{Py*} product and that the addition of an O-atom to the cyclohexenyl ring is associated with its cleavage.

In the case of the parent dG^{Py} adduct, fragmentation of the pyrimidine ring in the aglycone ion involves cleavage of the N^2 – C10 bond between the exocyclic NH_2 group and the pyrenyl residue to form $[GH]^+$ at *m/z* 152.2 and the pyrenyl fragment at *m/z* 303.1 (Figure S1, Supporting Information). In the case of 10*S* (+)-*trans-anti*-[Py]-N^2-8-oxodG we found an alternative pathway of fragmentation of the pyrimidine ring in the aglycone ion, which involves breakage of the C6 – N1 and C4 – N3 bonds to form the ions detected at *m/z* 362.1 and *m/z* 359.1 (Figure S2). The further fragmentation of the protonated free base, $[GH]^+$ (Figures 6, S1 and S2) involves cleavage of the C6 – N1 bond followed by a collapse of the ring-opened ion formed by two principal pathways: (1) expulsion of ammonia (NH_3) to form the ion at *m/z* 135.1, and (2) expulsion of CH_2N_2 fragment (as cyanamide, $NCNH_2$ or carbodiimide, HNCNH) to form the ion at m/z 110.1 (29). Assignment of the ions generated by fragmentation of the pyrenyl residues was made by comparison of the product ion spectra of the dG^{Py*} adduct (Figure 6), the parent 10*S* (+)-*trans-anti*-[Py]-N^2-dG adduct (Figure S1), the 10*S* (+)-*trans-anti*-[Py]-N^2-8-oxodG adduct (Figure S2), and 7,8,9,10-tetrahydroxytetrahydrobenzo[a]pyrene (Figure S3).

Proposed mechanism dG^{Py*} formation

Based on these cumulative results, we propose that the two-photon excitation of the pyrenyl residues of free 10*S* (+)-*trans-anti*-[Py]-N^2-dG nucleoside, or the same adduct embedded in oligonucleotides, induces a heterolytic cleavage of the “benzylic” C9-C10 (Figure 8) or C7-C8 bonds in the cyclohexenyl ring (25-27). In aqueous solutions the carbanion and carbocation-equivalent fragments formed in the primary photochemical step immediately react with water to form either the hydroxyalkyl-substituted amine **5** (Figure 8), or products with two terminal OH-groups (see, below). The hydroxyalkyll-substituted amine **5** is unstable and can either decay to form the intact guanine and aldehyde fragments, or undergo oxidation that results in adduct **1** containing the amide fragment instead of the amine in the parent dG^{Py}. The similar example of the amine to amide transformation is the oxidation of 2-(benzylideneamino)-2′-deoxyadenosine to 2-benzamido-2′-deoxyadenosine (31). Our experiments have shown that O_2 is not required for the generation of the dG^{Py*} product (18) and the most likely oxidizing agents that can serve as the electron acceptors in this step are the dG^{Py} radical cations that are generated by laser photoexcitation. In $H_2{}^{18}O$ solutions this pathway involves ^{18}O-atom addition to C10 and the transformation of **5** to the dG^{Py*}

product **1** containing one ^{18}O-atom (Figure 3A). However, the exact nature of the oxidant requires further investigation. This proposed pathway is supported by direct experiments: (1) the presence of one ^{18}O-atom in the dG^{Py*} photoproduct that is derived from in $H_2{}^{18}O$ (Figure 3A), and (2) the photodetachment of the Py-residues and the recovery of the intact guanine bases (18, 21). In contrast, pathways that involve O-atom addition to C7, C8 or C9 to form products with two terminal OH-groups, are less favorable than those resulting in the formation of the hydroxyalkyl-substituted amine **5**. The two terminal OH-groups are unstable and should rapidly transform to aldehyde groups, which can be further oxidized to carboxyl groups that result in products **2** – **4** (Figure 5). In $H_2{}^{18}O$ solutions these pathways should result in the insertion of two ^{18}O-atoms (the first ^{18}O-atom added after the heterolytic cleavage remains in the adduct with a probability of ~0.5 during formation of the aldehyde group, and the second ^{18}O-atom is added during oxidation of the aldehyde to the carboxyl group). However, our experiments show that only one ^{18}O-atom derived from $H_2{}^{18}O$ is present in the dG^{Py*} product (Figure 3A). Therefore, the formation of structures **2** – **4** containing carboxyl groups (Figure 5) is unlikely. Although the formation of adduct **1** can account for all of the experimental results, further experiments are required to achieve an unambiguous structural assignment. However, investigations along these lines were beyond the scope of this work.

The oxidation pathways depicted in Figure 8 limit the injection of holes into the DNA strand and thus diminish the yield of nucleobase oxidation at oligonucleotide sites distant from the site of the photosensitizer (18). Our results suggest that in DNA hole injection experiments and studies of hole migration in DNA, it is desirable to determine the fate of the photosensitizer moiety to ensure that the photofragmentation of the sensitizer itself does not yield any potentially mobile reactive intermediates that could also lead to secondary DNA damage.

Supplementary Material

Refer to Web version on PubMed Central for supplementary material.

Acknowledgments

This work was supported by the National Institutes of Health, Grants R01 CA110261 (for P.C.D.) and CA099194 (for N.E.G.) that supported the synthesis of the Py-modified nucleosides. The content is solely the responsibility of the authors and does not necessarily represent the official views of the National Institutes of Health. The (±)-7*r*,8t-dihydroxy-*t*8,9-epoxy-7,8,9,10-tetrahydrobenzo[*a*]pyrene was obtained from the National Cancer Institute Chemical Carcinogen Reference Standard Repository and is gratefully acknowledged. Components of this work were conducted in the Shared Instrumentation Facility at NYU that was constructed with support from a Research Facilities Improvement Grant (C06 RR-16572) from the National Center for Research Resources, National Institutes of Health. The acquisition of the ion trap mass spectrometer was supported by the National Science Foundation (CHE-0234863).

Abbreviations

Py	pyrene
dG^{Py}	10*S* (+)-*trans-anti*-[Py]-N^2-dG
***anti*-BPDE**	(+)-7*r*,8*t*-dihydroxy-9*t*,10*t*-epoxy-7,8,9,10-tetrahydrobenzo[*a*]pyrene
dIz	2-amino-5-[(2-deoxy-β-D-*erythro*pentofuranosyl) amino]-*4H*-imidazol-4-one
8-oxodG	8-oxo-7,8-dihydro-2′-deoxyguanosine

References

1. Phillips DH. Fifty years of benzo(a)pyrene. Nature. 1983; 303:468–472. [PubMed: 6304528]
2. Conney AH. Induction of microsomal enzymes by foreign chemicals and carcinogenesis by polycyclic aromatic hydrocarbons: G. H. A. Clowes Memorial Lecture. Cancer Res. 1982; 42:4875–4917. [PubMed: 6814745]
3. Cheng SC, Hilton BD, Roman JM, Dipple A. DNA adducts from carcinogenic and noncarcinogenic enantiomers of benzo[a]pyrene dihydrodiol epoxide. Chem. Res. Toxicol. 1989; 2:334–340. [PubMed: 2519824]
4. Weinstein IB, Jeffrey AM, Jennette KW, Blobstein SH, Harvey RG, Harris C, Autrup H, Kasai H, Nakanishi K. Benzo(a)pyrene diol epoxides as intermediates in nucleic acid binding in vitro and in vivo. Science. 1976; 193:592–595. [PubMed: 959820]
5. Geacintov NE, Cosman M, Hingerty BE, Amin S, Broyde S, Patel DJ. NMR solution structures of stereoisomeric covalent polycyclic aromatic carcinogen-DNA adducts: Principles, patterns, and diversity. Chem. Res. Toxicol. 1997; 10:111–146. [PubMed: 9049424]
6. Xie XM, Geacintov NE, Broyde S. Stereochemical origin of opposite orientations in DNA adducts derived from enantiomeric anti-benzo[a]pyrene diol epoxides with different tumorigenic potentials. Biochemistry. 1999; 38:2956–2968. [PubMed: 10074348]
7. Mocquet V, Kropachev K, Kolbanovskiy M, Kolbanovskiy A, Tapias A, Cai Y, Broyde S, Geacintov NE, Egly JM. The human DNA repair factor XPC-HR23B distinguishes stereoisomeric benzo[a]pyrenyl-DNA lesions. Embo J. 2007; 26:2923–2932. [PubMed: 17525733]
8. Xu P, Oum L, Geacintov NE, Broyde S. Nucleotide selectivity opposite a benzo[a]pyrene-derived N2-dG adduct in a Y-family DNA polymerase: A 5′-slippage mechanism. Biochemistry. 2008; 47:2701–2709. [PubMed: 18260644]
9. Geacintov NE, Cosman M, Mao B, Alfano A, Ibanez V, Harvey RG. Spectroscopic characteristics and site I/site II classification of cis and trans benzo[a]pyrene diolepoxide enantiomer-guanosine adducts in oligonucleotides and polynucleotides. Carcinogenesis. 1991; 12:2099–2108. [PubMed: 1934295]
10. Geacintov NE, Solntsev K, Johnson LW, Chen JX, Kolbanovskiy AD, Liu TM, Shafirovich VY. Photoinduced electron transfer and strand cleavage in pyrenyl-DNA complexes in adducts. J. Phys. Org. Chem. 1998; 11:561–565.
11. Geacintov NE, Zhao R, Kuzmin VA, Kim SK, Pecora LJ. Mechanisms of quenching of the fluorescence of a benzo[a]pyrene tetraol metabolite model compound by 2′-deoxynucleosides. Photochem. Photobiol. 1993; 58:185–194. [PubMed: 8415908]
12. Shafirovich VY, Courtney SH, Ya N, Geacintov NE. Proton-coupled photoinduced electron transfer, deuterium isotope effects, and fluorescence quenching in noncovalent benzo[a]pyrenetetraol-nucleoside complexes in aqueous solutions. J. Am. Chem. Soc. 1995; 117:4920–4929.
13. Shafirovich VY, Levin PP, Kuzmin VA, Thorgeirsson TE, Kliger DS, Geacintov NE. Photoinduced electron transfer and enhanced triplet yields in benzo[a]pyrene derivative-nucleic acid complexes and covalent adducts. J. Am. Chem. Soc. 1994; 116:63–72.
14. O'Connor D, Shafirovich VY, Geacintov NE. Influence of adduct stereochemistry and hydrogen-bonding solvents on photoinduced charge transfer in a covalent benzo[a]pyrene diol epoxide-nucleoside adduct on picosecond time scales. J. Phys. Chem. 1994; 98:9831–9839.
15. Kim SK, Geacintov NE, Brenner HC, Harvey RG. Identification of conformationally different binding sites in benzo[a]pyrene diol epoxide-DNA adducts by low-temperature fluorescence spectroscopy. Carcinogenesis. 1989; 10:1333–1335. [PubMed: 2500269]
16. Marsch GA, Jankowiak R, Suh M, Small GJ. Sequence dependence of benzo[a]pyrene diol epoxide-DNA adduct conformer distribution: A study by laser-induced fluorescence/polyacrylamide gel electrophoresis. Chem. Res. Toxicol. 1994; 7:98–109. [PubMed: 8155833]
17. Pradhan P, Jernstrom B, Seidel A, Norden B, Graslund A. Induced circular dichroism of benzo[a]pyrene-7,8-dihydrodiol 9,10-epoxide stereoisomers covalently bound to deoxyribooligonucleotides used to probe equilibrium distribution between groove binding and intercalative adduct conformations. Biochemistry. 1998; 37:4664–4673. [PubMed: 9521787]

18. Yun BH, Lee YA, Kim SK, Kuzmin V, Kolbanovskiy A, Dedon PC, Geacintov NE, Shafirovich V. Photosensitized oxidative DNA damage: from hole injection to chemical product formation and strand cleavage. J. Am. Chem. Soc. 2007; 129:9321–9332. [PubMed: 17616188]
19. Kuzmin VA, Dourandin A, Shafirovich V, Geacintov NE. Proton-coupled electron transfer in the oxidation of guanines by an aromatic pyrenyl radical cation in aqueous solutions. Phys. Chem. Chem. Phys. 2000; 2:1531–1535.
20. Burrows CJ, Muller JG. Oxidative nucleobase modifications leading to strand scission. Chem. Rev. 1998; 98:1109–1151. [PubMed: 11848927]
21. Li B, Mao B, Liu TM, Xu J, Dourandin A, Amin S, Geacintov NE. Laser pulse-induced photochemical strand cleavage of site-specifically and covalently modified (+)-anti-benzo[a]pyrene diol epoxide-oligonucleotide adducts. Chem. Res. Toxicol. 1995; 8:396–402. [PubMed: 7578926]
22. Sigman ME, Schuler PF, Ghosh MM, Dabestani RT. Mechanism of pyrene photochemical oxidation in aqueous and surfactant solutions. Environ. Sci. Technol. 1998; 32:3980–3985.
23. Harada, N.; Nakanishi, K. Circular Dichroic Spectroscopy: Exciton Coupling in Organic Stereochemistry. University Science Books; Mill Valley, CA: 1983.
24. Nakanishi K, Kasai H, Cho H, Harvey RG, Jeffrey AM, Jennette KW, Weinstein AB. Absolute configuration of a ribonucleic acid adduct formed in vivo by metabolism of benzo[a]pyrene. Absolute configuration of a ribonucleic acid adduct formed in vivo by metabolism of benzo[a]pyrene. J. Am. Chem. Soc. 1977; 99:258–260. [PubMed: 830680]
25. Margerum JD, Petrusis CT. The photodecarboxylation of nitrophenylacetate Ions. J. Am. Chem. Soc. 1969; 91:2467–2472.
26. Krogh E, Wan P. General method for the photogeneration of benzolated cationic and anionic systems in aqueous solution. Test of relative stability of these systems in the excited state. Tetrahedron Lett. 1986; 27:823–826.
27. Wan P, Muralidharan S. Structure and mechanism in the photo-retro-aldol type reactions of nitrobenzyl derivatives. photochemical heterolytic cleavage of C-C bonds. J. Am. Chem. Soc. 1988; 110:4336–4345.
28. Xu M, Lukeman M, Wan P. Photodecarboxylation of benzoyl-substituted biphenylacetic acids and photo-retro-aldol reaction of related compounds in aqueous solution. Acid and base catalysis of reaction. J. Photochem. Photobiol. A. 2009; 204:52–62.
29. Gregson JM, McCloskey JA. Collision-induced dissociation of protonated guanine. Int. J. Mass Spectrom. 1997; 165/166:475–485.
30. Bessette EE, Goodenough AK, Sophie Langoue S, Isil Yasa I, Kozekov ID, Spivack SD, Turesky RJ. Screening for DNA adducts by data-dependent constant neutral loss-triple stage mass spectrometry with a linear quadrupole ion trap mass spectrometer. Anal. Chem. 2009; 81:809–819. [PubMed: 19086795]
31. Kuttappan-Nair V, Samson-Thibault F, Wagner JR. Generation of 2′-deoxyadenosine N6-aminyl radicals from the photolysis of phenylhydrazone derivatives. Chem. Res. Toxicol. 2010; 23:48–54. [PubMed: 20000474]

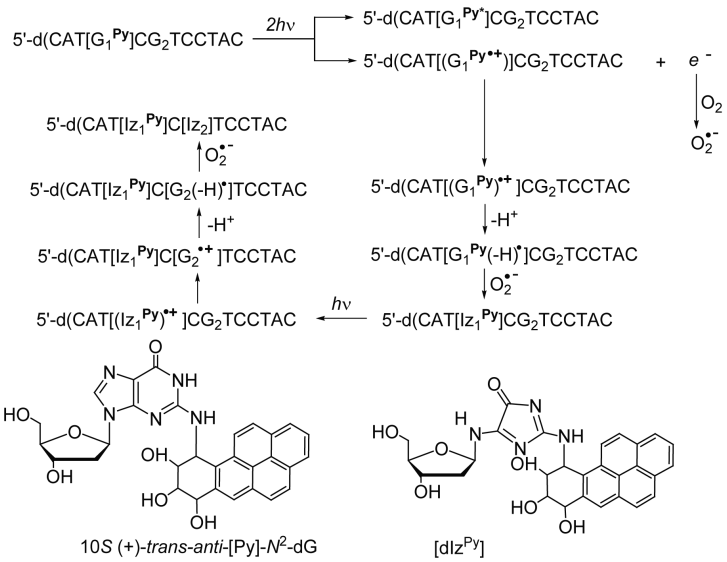

Figure 1.

Photochemical damage of 10*S* (+)-*trans-anti*-[Py]-N^2-dG adducts site-specifically positioned in the oligonucleotide sequence (18). dG_1^{Py*} is M+16 lesion.

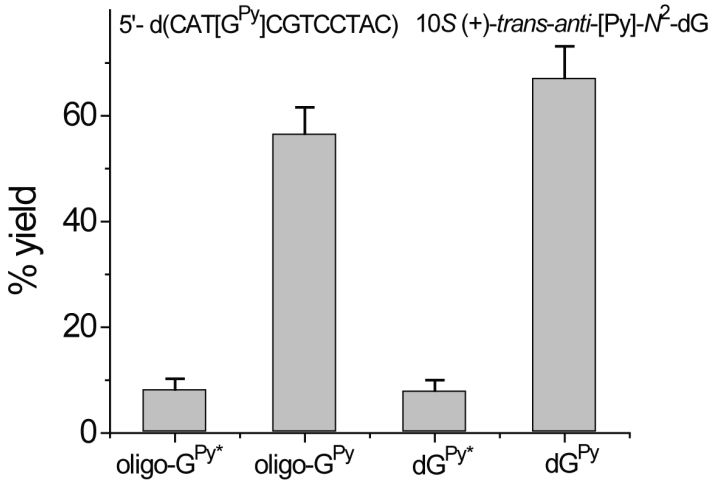

Figure 2.

Yields of the M+16 product dG^{Py*} resulting from the laser flash photolysis of the d(CAT**[G_1^{Py}]CG_2**TCCTAC) sequence and after its complete enzymatic digestion to the nucleoside level (from the data of Yun et al.(18)), or the nucleoside adduct dG^{Py},10*S* (+)-*trans-anti*-[Py]-N^2-dG adduct (this work), The experiments were conducted in air-equilibrated phosphate buffer solutions (pH 7.0) and irradiation by a train of 355 nm laser flash pulses (4 mJ/cm^2, 10Hz) for 20 s.

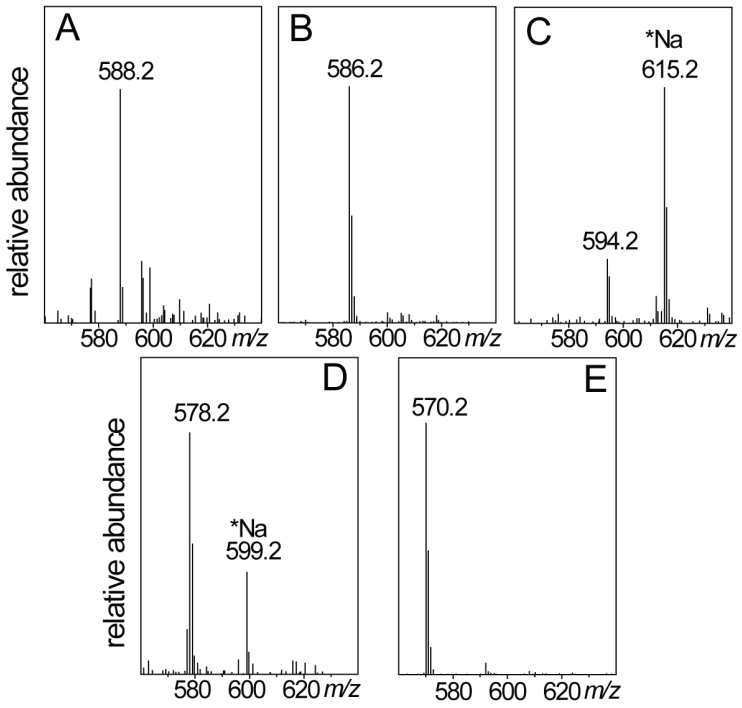

Figure 3.

Positive ion spectra of the dG^{Py*} adducts generated by photolysis of 10*S*(+)-*trans*-*anti*-[Py]-N^2-dG. (A) The dG^{Py*} adduct synthesized in $H_2{}^{18}O$ buffer solutions (mass M+18). (B) The dG^{Py*} adduct synthesized in $H_2{}^{16}O$ buffer solutions (mass M+16). (C) The dG^{Py*} adduct in D_2O. (D) The dG^{Py} in D_2O. (E) The dG^{Py} adduct in $H_2{}^{16}O$ (mass M). The spectra were recorded using 0.1% formic acid in H_2O/CH_3CN = 1 : 1 v/v mixtures (A, B and E), and 0.1% formic acid in D_2O/CH_3CN 1 : 1 v/v (C and D) mobile phases, respectively. In D_2O mobile phases, the *m/z* values of sodium adducts (*Na) are greater by 21 Da than those of the corresponding molecular ions.

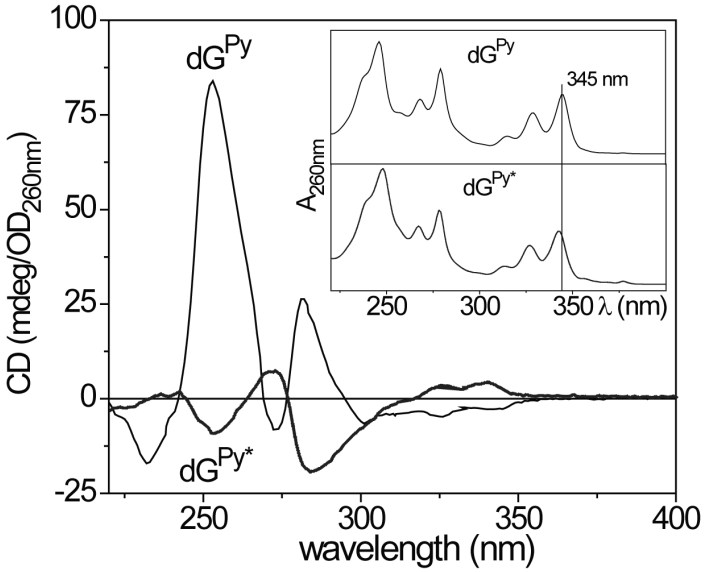

Figure 4.

The circular dichroism spectra of the 10*S* (+)-*trans-anti*-[Py]-N^2-dG (dG^{Py}) precursor adduct and the M+ 16 dG^{Py*} oxidation product. Inset: Absorption spectra of the dG^{Py} and dG^{Py*} adducts.

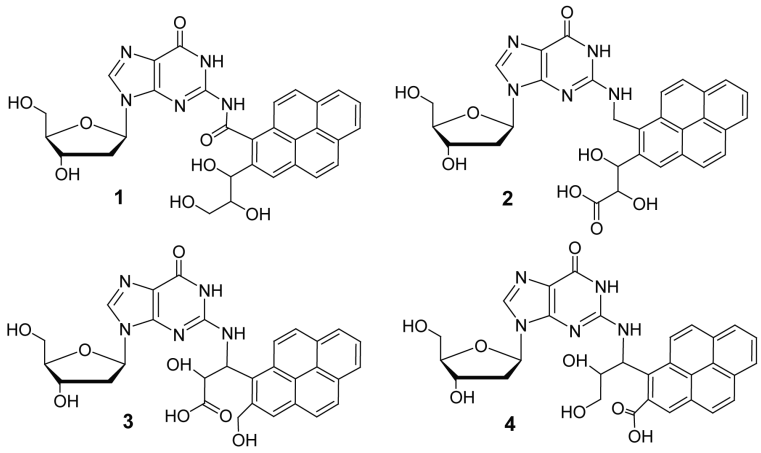

Figure 5.
Proposed structures of dG^{Py*} adduct produced by the rupture of the cycloxenyl ring.

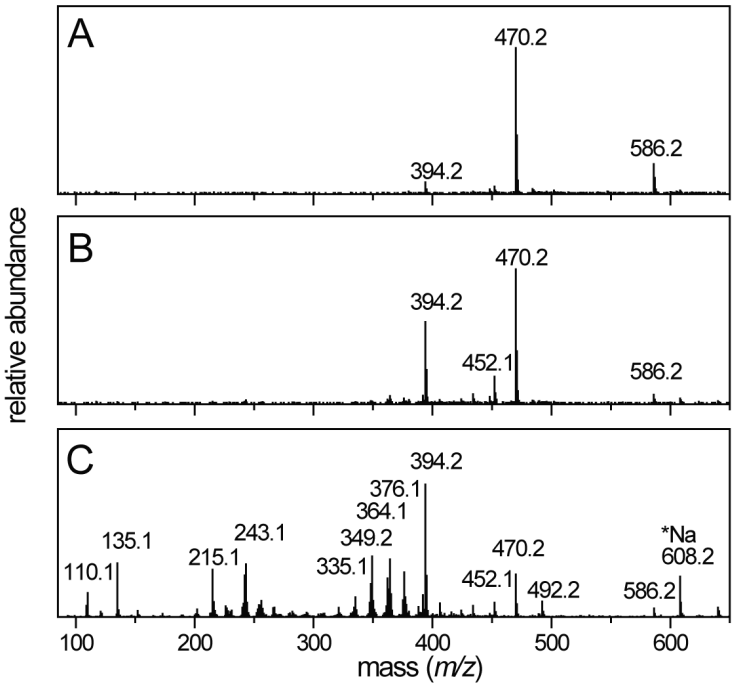

Figure 6.
Positive product ion spectra of the dG^{Py*} adduct recorded at different fragmentor voltages (A) 90 V, (B) 130V, and (C) 190 V.

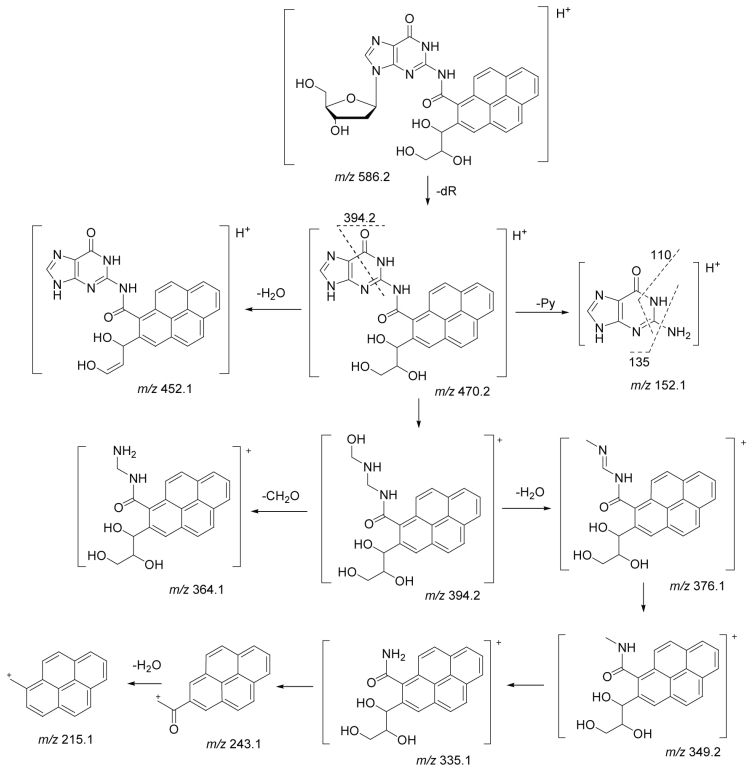

Figure 7.
Fragmentation pathways of molecular and daughter ions of the dG^{Py*} adduct.

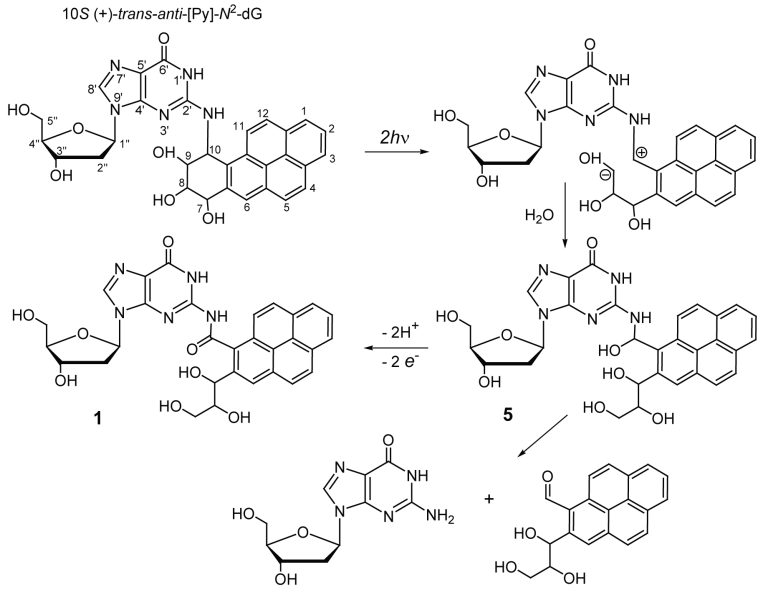

Figure 8.
Proposed mechanism of M+16 product o formation.